

# Generating high-order exceptional points in coupled electronic oscillators using complex synthetic gauge fields

José D. Huerta-Morales,<sup>1,\*</sup> Mario A. Quiroz-Juárez,<sup>2</sup> Yogesh N. Joglekar,<sup>3,†</sup> and Roberto de J. León-Montiel<sup>1,‡</sup>

<sup>1</sup>*Instituto de Ciencias Nucleares, Universidad Nacional Autónoma de México,  
Apartado Postal 70-543, 04510 Cd. Mx., México*

<sup>2</sup>*Centro de Física Aplicada y Tecnología Avanzada, Universidad Nacional Autónoma de México,  
Boulevard Juriquilla 3001, 76230 Querétaro, México*

<sup>3</sup>*Department of Physics, Indiana University - Purdue University Indianapolis (IUPUI), Indianapolis, Indiana 46202 USA*

(Dated: February 15, 2023)

Exceptional points (EPs) are degeneracies of non-Hermitian systems, where both eigenvalues and eigenvectors coalesce. Classical and quantum systems exhibiting high-order EPs have recently been identified as fundamental building blocks for the development of novel, ultra-sensitive opto-electronic devices. However, arguably one of their major drawbacks is that they rely on non-linear amplification processes that could limit their potential applications, particularly in the quantum realm. In this work, we show that high-order EPs can be designed by means of linear, time-modulated, chain of inductively coupled RLC (where R stands for resistance, L for inductance, and C for capacitance) electronic circuits. With a general theory, we show that  $N$  coupled circuits with  $2N$  dynamical variables and time-dependent parameters can be mapped onto an  $N$ -site, time-dependent, non-Hermitian Hamiltonian, and obtain constraints for  $\mathcal{PT}$ -symmetry in such models. With numerical calculations, we obtain the Floquet exceptional contours of order  $N$  by studying the energy dynamics in the circuit. Our results pave the way toward realizing robust, arbitrary-order EPs by means of synthetic gauge fields, with important implications for sensing, energy transfer, and topology.

## I. INTRODUCTION

The past two decades have witnessed a Cambrian explosion of several experimental and theoretical investigations on non-Hermitian Hamiltonian systems that satisfy the so-called parity-time ( $\mathcal{PT}$ ) symmetry condition [1–5]. Owing to the antilinear  $\mathcal{PT}$ -symmetry, the spectrum of such Hamiltonians changes from real to complex-conjugate pairs as the degree of anti-Hermiticity is increased. The coherent, non-unitary evolution generated by the non-Hermitian Hamiltonian means that the norm of a state oscillates in the  $\mathcal{PT}$ -symmetric region, where the spectrum is real, and grows exponentially in the  $\mathcal{PT}$ -broken region, where amplifying (and decaying) eigenmodes are present. The study and analysis of  $\mathcal{PT}$ -symmetric systems across the parameter domain have triggered important theoretical predictions and experimental demonstrations in disparate areas of physics, optics, and photonics [6–9]. Specifically, the non-trivial phenomena across the  $\mathcal{PT}$ -transition have captured a great deal of attention. This is, in part, because the exceptional-point degeneracy—in contrast with the traditional Hermitian degeneracy—is a potentially good candidate for sensing small disturbances due to a perturbing potential [10–16].

For Hermitian Hamiltonians, however, even when two eigenvalues become degenerate, two orthonormal eigenvectors remain. Exceptional points (EPs) are thus non-Hermitian singularities where two or more eigenvectors

also coalesce [17–19]. The number of eigenvectors  $n$  that collapse at the non-Hermitian degeneracy defines the order of the EP, and we call it,  $\text{EP}n$ . The most common case is an  $\text{EP}2$ , where a pair of eigenvalues become degenerate, and EPs of order greater than two are traditionally referred to as high-order EPs [20–23]. The literature on the design and realization of high-order EPs has greatly contributed to the development of this research field, most of them aimed at enhancing the response of open physical systems [24, 25] because the dimensionless mode-splitting  $\Delta\omega$  in response to a dimensionless perturbation  $\delta \ll 1$  at an  $\text{EP}n$  is given by  $\Delta\omega(\delta) \propto \delta^{1/n} \gg \delta$ . Put simply, the sensitivity to perturbations increases as the order of the EP increases. For instance, a 1% perturbation results in a 1% response in a Hermitian system, a 10% response at an  $\text{EP}2$ , and a 30% response at an  $\text{EP}3$ .

Recent theoretical and experimental studies have focused on diverse  $\mathcal{PT}$ -symmetric platforms to realize EPs of arbitrary order. Examples include waveguide-arrays [7, 9, 26], micro-cavities [13, 14, 27], opto-mechanical systems [28–30], quantum optical circuits [31, 32], coupled acoustic resonators [33–35], and electronic circuits [12, 36–39]. The latter, in recent years, have emerged as a powerful platform for simulating topological and non-Hermitian phenomena [40–42]. In particular, we have shown that both gain and loss can be implemented in a single LC oscillator by means of synthetic gauge fields, thereby creating static and Floquet  $\text{EP}2$  landscape [43]. Extending this approach to higher-dimensional EPs is, however, non-trivial.

In this work, we show through analytical and numerical methods that it is possible to engineer high-order EPs in an inductively-coupled RLC-circuit tight-binding lattice. We use the  $J_y$  array—a tight binding lattice with non-

\* jose.huerta@correo.nucleares.unam.mx

† yojoglek@iupui.edu

‡ roberto.leon@nucleares.unam.mx

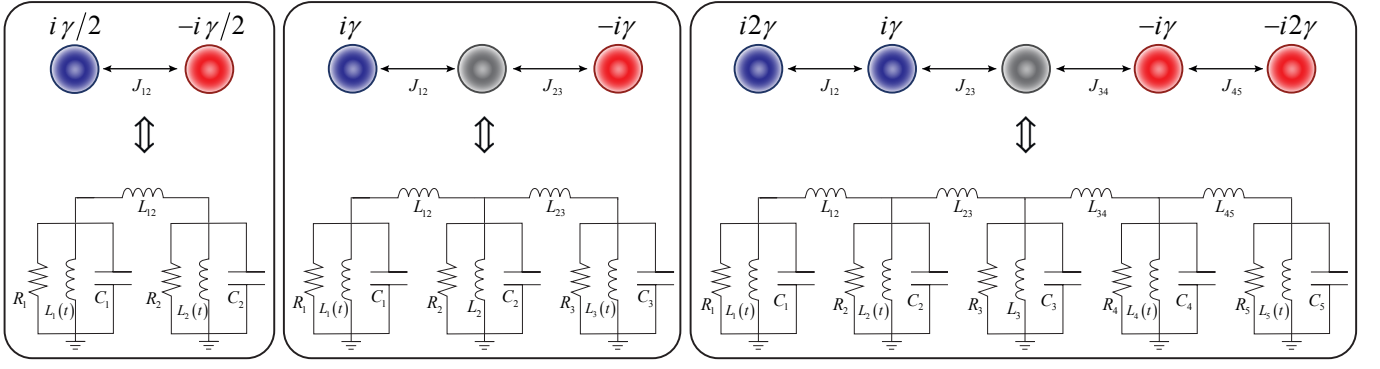


Figure 1. **Schematic representation of the equivalence between sites and electronic circuits in a tight-binding lattice model.** The top row shows  $\mathcal{PT}$ -symmetric perfect-state-transfer lattice with  $N = 2, 3, 5$  sites respectively. Its Hamiltonian  $H_N(\gamma) = \kappa J_y + i\gamma J_z$  is  $N$  dimensional. Bottom row shows  $N$  inductively coupled RLC circuits with  $2N$  dynamical variables, exhibiting synthetic gain and loss by means of time-dependent inductance within each RLC box.

uniform couplings that has equidistant eigenvalues [44–46] – along with a gain-loss profile that mimics the  $J_z$  array to realize higher-order EPs [19]. Specifically, we implement the non-trivial features of  $\mathcal{PT}$ -symmetry with synthetic gain and loss through the temporal variation of the inductances in each oscillator [38, 39, 43]. Our results suggest that dynamically tunable synthetic electronics, with  $\mathcal{PT}$ -symmetry implemented through a complex gauge field, can be used to simulate higher-order EPs.

The paper is organized as follows. In Sec. II we present the formalism that maps the Kirchoff-law equations for currents and voltages in a chain of  $N$  inductively coupled RLC oscillators into a Schrodinger-like equation with a  $N_e \equiv (3N - 1)$  dimensional Hamiltonian, and show how a time-dependent, non-unitary change of basis can lead to gain and loss. In Sec. III we demonstrate that the time-modulation of specific components of those oscillators can create EPN contours. Section IV provides a brief discussion and conclusions. The explicit forms of the Hamiltonians for  $N = 3, 4, 5$  are given in the Appendix.

## II. THE MODEL

Let us consider a set of  $N$  RLC circuits connected by  $(N - 1)$  coupling inductors (Fig. 1). Their dynamics are governed by the following first-order equations [47]

$$\frac{dV_n}{dt} = \frac{1}{C_n} \left[ -\frac{V_n}{R_n} - I_n - I_{x,n} + I_{x,n-1} \right], \quad (1a)$$

$$\frac{dI_n}{dt} = \frac{1}{L_n} V_n, \quad (1b)$$

$$\frac{dI_n^x}{dt} = \frac{1}{L_{x,n}} (V_n - V_m). \quad (1c)$$

These equations arise from the Kirchoff laws. Here,  $V_n(t)$  is the voltage in the capacitor  $C_n$ ,  $I_n(t)$  is the current across the inductor  $L_n$ ,  $R_n$  is the resistance in

the  $n$ th oscillator,  $L_{x,n}$  denotes the inductor coupling the  $n$ th RLC box to the  $(n+1)$ th box, and  $I_{x,n}(t)$  is the current flowing across it. We can write the  $N_e \equiv (3N - 1)$  Eqs. (1a)-(1c) in a compact form as

$$i \frac{d}{dt} |\phi(t)\rangle = H(t) |\phi(t)\rangle, \quad (2)$$

where the  $N_e$ -dimensional “state-vector” is

$$|\phi(t)\rangle = (V_1, \dots, V_N, I_1, \dots, I_N, I_{x,1}, \dots, I_{x,N-1})^T \quad (3)$$

$H(t)$  is a non-Hermitian,  $N_e \times N_e$  matrix with purely imaginary entries. To specify its general structure, we define ancillary matrices  $\mathbb{C} = \text{diag}(C_1, \dots, C_N)$ ,  $\mathbb{L} = \text{diag}(L_1, \dots, L_N)$ ,  $\mathbb{G}_{RC} = \text{diag}(1/R_1 C_1, \dots, 1/R_N C_N)$ , and  $\mathbb{L}_x = \text{diag}(L_{x,1}, \dots, L_{x,N-1})$ . Additionally, we also define an  $N \times (N - 1)$ , almost skew-symmetric matrix  $\mathbb{S}$  with entries  $\mathbb{S}_{ab} = \delta_{ab} - \delta_{a,b+1}$ . In terms of these matrices,  $H$  can be written as

$$H = i \begin{bmatrix} -\mathbb{G}_{RC} & -\mathbb{C}^{-1} & -\mathbb{C}^{-1}\mathbb{S} \\ \mathbb{L}^{-1} & 0 & 0 \\ \mathbb{L}_x^{-1}\mathbb{S}^\dagger & 0 & 0 \end{bmatrix}. \quad (4)$$

Since the state vector  $|\phi(t)\rangle$  has entries with different engineering dimensions, so does the matrix  $H$ . To clarify its underlying symmetry properties, it is useful to consider the “square-root-of-energy” basis. The energy in the  $N$ -node circuit is given by

$$\begin{aligned} E(t) &= \frac{1}{2} \sum_{n=1}^N [C_n V_n^2 + L_n I_n^2] + \frac{1}{2} \sum_{m=1}^{(N-1)} L_{x,m} I_{x,m}^2 \\ &= \langle \phi(t) | A | \phi(t) \rangle, \end{aligned} \quad (5)$$

where the positive,  $N_e$  dimensional bilinear-form matrix is given by  $A = \text{diag}(\mathbb{C}, \mathbb{L}, \mathbb{L}_x)/2$ . We define  $|\psi(t)\rangle = A^{1/2}(t)|\phi(t)\rangle$  so that norm of  $|\psi(t)\rangle$  encodes the circuit energy,  $\langle \psi(t) | \psi(t) \rangle = E(t)$ . Note that all entries in the state vector  $|\psi(t)\rangle$  have units of  $\sqrt{\text{Joules}}$ . It is straightforward to show that  $|\psi(t)\rangle$  satisfies a Schrödinger-like

equation

$$i \frac{d}{dt} |\psi(t)\rangle = (H_0 + \Gamma) |\psi(t)\rangle = H_{\text{cir}}(t) |\psi(t)\rangle, \quad (6)$$

where the effective circuit Hamiltonian  $H_{\text{cic}} = H_0 + \Gamma$  has two components. The first component  $H_0$  is given by

$$H_0 = \sqrt{A} H \frac{1}{\sqrt{A}} = i \begin{bmatrix} -\mathbb{G}_{RC} & -\mathbb{W} & -\frac{1}{\sqrt{C}} \mathbb{S} \frac{1}{\sqrt{L_x}} \\ \mathbb{W} & 0 & 0 \\ \frac{1}{\sqrt{L_x}} \mathbb{S}^\dagger \frac{1}{\sqrt{C}} & 0 & 0 \end{bmatrix} \quad (7)$$

where  $\mathbb{W} = \text{diag}(\omega_1, \dots, \omega_N)$  is a diagonal matrix with frequencies of individual oscillators  $\omega_k = 1/\sqrt{C_k L_k}$ . When there is no dissipation in each  $RLC$  circuit, i.e.  $\mathbb{G}_{RC} = 0$ , the matrix  $H_0$  becomes Hermitian and the corresponding unitary evolution of the state  $|\psi(t)\rangle$  signals the conservation of total energy in the circuit. When  $\mathbb{G}_{RC} > 0$ , this anti-Hermitian piece of  $H_0$  encodes the Joule dissipation. The second component of  $H_{\text{cic}}$  is given by

$$\Gamma(t) = i \frac{1}{\sqrt{A}} \frac{d}{dt} \sqrt{A} = i \frac{d}{dt} \ln \sqrt{A(t)}. \quad (8)$$

If the change of basis matrix  $\sqrt{A(t)}$  is unitary, as is typically the case, its spatiotemporal variations give rise to a Hermitian  $\Gamma(t)$  since the logarithm of a unitary matrix is an anti-Hermitian matrix. However, as our change of basis matrix  $A = \text{diag}(C, \mathbb{L}, \mathbb{L}_x)/2$  is not unitary and always real, it leads to an anti-Hermitian, gain-loss term  $\Gamma(t)$ , as defined in Eq. (8).

The parity operator exchanges the node  $n$  with its mirror symmetric node  $\bar{a} = N + 1 - a$ . Therefore, it is given by  $\mathcal{P} = \text{diag}(\Pi_N, \Pi_N, -\Pi_{N-1})$  where  $\Pi_k = \Pi_k^{-1} = \Pi_k^\dagger$  is the antidiagonal matrix of size  $k$  with unit entries. The time-reversal operator, in addition to the complex-conjugation operation  $*$ , reverses the sign of each current:  $\mathcal{T} = \text{diag}(\mathbb{1}_N, -\mathbb{1}_N, -\mathbb{1}_{N-1})^*$ . Thus, the antilinear  $\mathcal{PT}$  operator is given by the following  $N_e$ -dimensional, block-diagonal matrix

$$\mathcal{PT} = \text{diag}(\Pi_N, -\Pi_N, \Pi_{N-1})^* = \mathcal{U}^*, \quad (9)$$

where  $\mathcal{U}$  denotes the  $N_e$ -dimensional real, unitary matrix. By imposing the constraint that  $H_0$  is  $\mathcal{PT}$ -symmetric, we get

$$\Pi_N \mathbb{G}_{RC} \Pi_N = -\mathbb{G}_{RC} = 0, \quad (10)$$

$$\Pi_N \mathbb{W} \Pi_N = \mathbb{W}, \quad (11)$$

$$\Pi_N \frac{1}{\sqrt{C}} \mathbb{S} \frac{1}{\sqrt{L_x}} = \frac{1}{\sqrt{C}} \mathbb{S} \frac{1}{\sqrt{L_x}} \Pi_{N-1}. \quad (12)$$

Equivalently, these conditions mean no resistive losses,  $\omega_a = \omega_{\bar{a}}$ , and  $C_a L_{x,a} = C_{\bar{a}} L_{x,\bar{a}}$ . Similarly, requiring  $\mathcal{PT}$  symmetry for the anti-Hermitian potential implies  $\mathcal{P}A\mathcal{P} = A$  or equivalently,  $C_a = C_{\bar{a}}$ ,  $L_a = L_{\bar{a}}$ , and  $L_{x,a} = L_{x,N-a}$ .

Next, we outline the mapping of this  $N_e$ -dimensional dynamical system onto an  $N$ -dimensional tight-binding model. Since  $H_0$  has purely imaginary entries, for a  $\mathcal{PT}$ -symmetric Hamiltonian, the unitary  $\mathcal{U}$  in Eq. (9) anti-commutes with it. Therefore, the eigenvalues of  $H_0$  occur in pairs  $\pm \epsilon_a$ , or equivalently, it has a chiral symmetry. It also follows, most clearly from Eq. (7), that  $H_0$  has  $(N - 1)$  linearly-dependent columns and therefore  $(N - 1)$  eigenvalue zeros. This combination of chiral symmetry and zero modes is instrumental to mapping the  $N_e = (3N - 1)$  dimensional system onto an  $N$ -dimensional model. These arguments remain valid when a  $\mathcal{PT}$ -symmetric complex gauge potential  $\Gamma$  is added, and therefore, the  $\mathcal{PT}$ -symmetric circuit Hamiltonian  $H_{\text{cic}}$  of size  $N_e$  can always be mapped onto a  $\mathcal{PT}$ -symmetric tight-binding model with  $N$  sites.

The canonical model with an exceptional point of order  $N$  is  $H(\gamma) = \kappa J_x + i\gamma J_z$  where  $J_x, J_z$  are  $N$  dimensional representations of  $\text{su}(2)$  [19, 21, 44, 48]. However, because we have a classical system with a purely real state vector, we use its counterpart with purely imaginary entries,  $H_N(\gamma) = \kappa J_y + i\gamma J_z$ . In such tight-binding lattice, the Hermitian coupling between adjacent sites is given by  $J_y(a, a + 1) = i\sqrt{a(N + 1 - a)}/2 = -J_y(a + 1, a)$ . Now, to connect the  $J_y$  matrix elements to our coupled electrical circuits model, we use the expression for the effective, dimensionless tunneling amplitude between two inductively coupled circuits,  $J_{\text{eff}} = M^2/2\sqrt{1 + M^2}$  where  $M^2 = L/L_x$  [49].

Similarly, to create the gain-loss term  $i\gamma(t)J_z$  the inductors  $L_a(t)$  within each circuit are modulated while keeping the capacitors and coupling inductors static across the array. Since  $J_z = \text{diag}(s, s - 1, \dots, -s)$  where  $s = (N - 1)/2$  is the spin associated with the  $N$ -dimensional representation, using the modulation

$$L_a(t) \equiv L_0 e^{f_a(t)} = L_0 e^{(N+1-2a) \int_0^t \gamma(t') dt'}, \quad (13)$$

leads to  $\Gamma = i\gamma(t)\text{diag}(0_N, J_z, 0_{N-1})$ . This temporal variation means the inductors in mirror-symmetric positions are varied in an inverse manner,  $L_a(t)L_{\bar{a}}(t) = L_0^2 = \text{const}$ . Therefore, when inductance increase at site  $a$ , indicating gain, is balanced by inductance decrease at its mirror symmetric site  $\bar{a}$ , indicating loss,

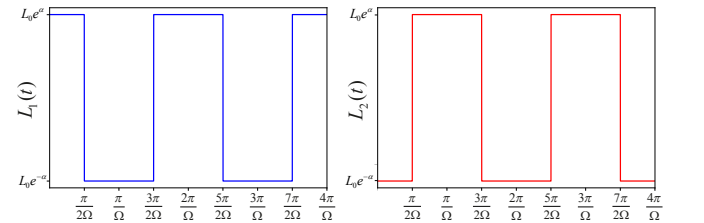


Figure 2. **Square-wave periodic function with modulation frequency  $\Omega$ .** (a) For  $N = 2$ , the time-dependent inductances are given by  $L_1(t) = L_0 e^{f(t)}$ . (b) shows the complementary,  $L_2(t) = L_0 e^{-f(t)} = L_0^2/L_1(t)$ .

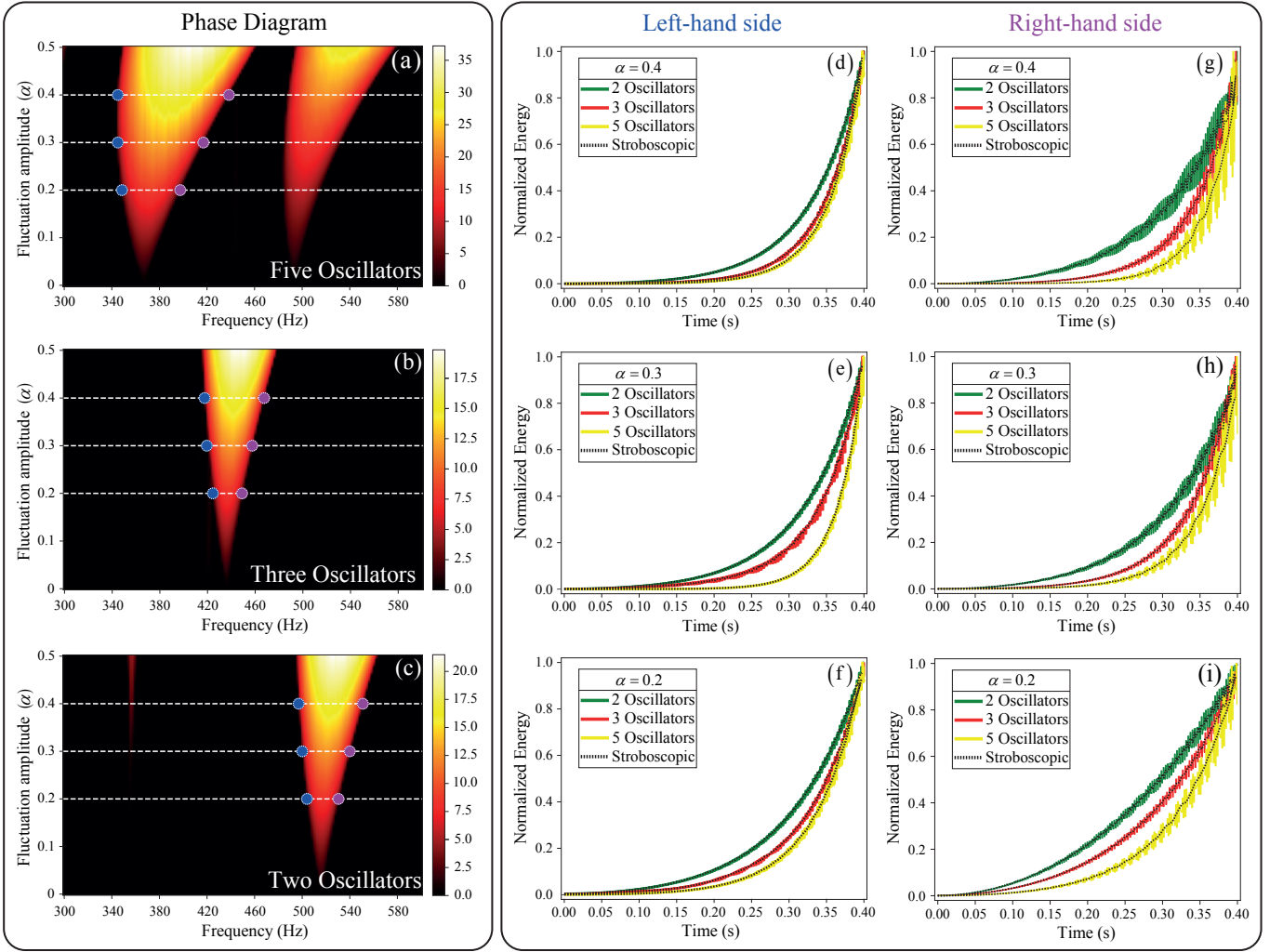


Figure 3. **High-order EP contours in the  $(\alpha, \Omega)$  plane.** (a)-(c)  $\mu(\alpha, \omega)$  in the frequency window from  $\Omega/(2\pi) = 300$  Hz to 600 Hz is obtained using  $\tau = 100$  ms. The EP contours, separating regions from light windows, are clearly seen, with EPs along the  $\alpha = \{0.2, 0.3, 0.4\}$  lines shown as blue (left) and purple (right) filled circles. (d)-(f) normalized energy  $E(t)/E_{\max}$  for blue EPs on the left-side contour shows power-law in time growth, with an exponent determined by  $N$ , but independent of  $\alpha$ . Results for two, three, and five oscillators are shown in green, red, and yellow lines, respectively; overlaid black-dashed lines show stroboscopic results. (g)-(i) corresponding results for the purple EPs on the right-side contour, shown with the same conventions, are quantitatively similar.

and  $\mathcal{PT}$  symmetry can be created without real amplifying or Joule-heating elements. The exponent function  $f(t) = \int \gamma(t')dt'$  in Eq. (13) allows us to create arbitrary, balanced gain-loss profiles.

The choice of  $f(t)$  is informed by the ability to dynamically modulate the synthetic inductances in real time by using electronic circuits [43]. Creating a static gain-loss term requires inductances that either grow or decay exponentially [43]. However, Floquet EP contours of the same order also emerge by periodic variations [43, 49, 50]. For simplicity, we consider the square-wave function

$$f(t) = \begin{cases} \alpha & 0 \leq t \leq T/4, \\ -\alpha & T/4 < t \leq 3T/4, \\ \alpha & 3T/4 < t \leq T, \end{cases} \quad (14)$$

where  $T$  is the period and  $\Omega = 2\pi/T$  defines the modulation frequency. For example, when  $N = 2$ , the two inductances satisfy  $e^{-\alpha} \leq L_{1,2}(t)/L_0 \leq e^{\alpha}$  (Fig. 2). Since the inductance in each RLC box varies with time, the Hamiltonian  $H_0$  also acquires time-dependence through the matrix  $\mathbb{W}$  of frequencies  $\omega_a(t) = 1/\sqrt{L_a(t)C_a}$ .

The  $\mathcal{PT}$  phase diagram of this system can be obtained via two methods. The first uses the non-unitary time evolution operator  $G_F(T)$  to calculate the equivalent non-Hermitian,  $\mathcal{PT}$ -symmetric Floquet Hamiltonian  $G_F(T) \equiv \exp[-iH_F(\alpha, \Omega)T]$  [50]. The second, experimentally friendly approach is to obtain the time-dependent circuit energy  $E(t)$ , Eq. (5), and compare its growth over sufficiently long time-intervals  $\tau$  and  $2\tau$ . To

quantify it, we define a dimensionless ratio [43, 49]

$$\mu = \log \left\{ \frac{\max[E(0 \leq t \leq 2\tau)]}{\max[E(0 \leq t \leq \tau)]} \right\}. \quad (15)$$

In the  $\mathcal{PT}$ -symmetric phase with time-periodic dynamics,  $\max E(t)$  will be the same over the two intervals, and therefore  $\mu = 0$  denotes the  $\mathcal{PT}$ -symmetric phase. On the other hand, in  $\mathcal{PT}$ -broken phase with exponentially amplifying modes, Eq. (15) provides a linear-in- $\tau$  metric that indicates the average amplification  $\mu > 0$ . The  $\mathcal{PT}$  transition is accompanied by a vanishing energy gap and divergent period on the  $\mathcal{PT}$ -symmetric side of the boundary. Therefore, at any finite  $\tau$ , this approach leads to some smearing of the EP contours. In the following section, we present the results of such an analysis.

### III. RESULTS

For numerical analysis, we use experimentally accessible and viable circuit parameters [43]: resistance  $R_0 = 1$  k $\Omega$ , inductance  $L_0 = 0.01$  H and capacitance  $C_0 = 100$   $\mu$ F. Thus, the isolated oscillator frequency is  $\omega_0/(2\pi) = 159.15$  Hz, and the isolated oscillator RC-decay rate,  $1/R_0C_0 = 10$  Hz, is much smaller than the natural frequency, thereby justifying the approximation  $\mathbb{G}_{RC} \approx 0$ . The coupling inductances are set to  $L_{x1} = 0.5L_0$  for  $N = 2$  oscillators,  $L_{x1} = L_{x2} = 0.5L_0$  for  $N = 3$  oscillators, and  $L_{x1} = L_{x4} = 0.67L_0$ ,  $L_{x2} = L_{x3} = 0.5L_0$  for  $N = 5$  as necessitated by the non-uniform matrix elements of the  $J_y$  array. We use  $\alpha \leq 0.4$ , meaning the inductances span  $0.67L_0 \leq L_a(t) \leq 1.5L_0$ , a range that can be dynamically achieved in the synthetic circuits [43, 49].

The left-hand panel in Fig. 3 shows the numerically computed  $\mu(\alpha, \Omega)$  for  $N = 5$  (a),  $N = 3$  (b), and  $N = 2$  (c) over a modulation-frequency window  $\Omega/(2\pi)$  from 300 Hz to 600 Hz. The dark regions with  $\mu = 0$  denote the  $\mathcal{PT}$ -symmetric phase, where the circuit energy  $E(t)$  undergoes bounded oscillations. They are punctuated by bright, triangular,  $\mathcal{PT}$ -symmetry broken regions ( $\mu > 0$ ) that occur down to vanishingly small non-Hermiticity  $\alpha \ll 1$  at specific frequencies [43, 49, 50]. These regions are separated by EP contours with order  $N$ .

We analyze the dynamics at the EPs by monitoring how fast the circuit energy  $E(t)$  increases when the system is parked at the EPs (shown by blue, left and purple, right circles with white boundaries) along  $\alpha = \{0.2, 0.3, 0.4\}$  lines. The center panel in Fig. 3 shows normalized energies  $E(t)/E_{\max}$  (solid lines) and their respective stroboscopic results (black-dashed lines) at  $\alpha = 0.4$  (d),  $\alpha = 0.3$  (e), and  $\alpha = 0.2$  (f) when the system is parked on the blue, left EPs. Figure 3 (g)-(i) show corresponding results when the system is parked on the purple, left EPs. In each case, it can be seen that  $E(t)/E_{\max}$  follows a power-law dependence on  $t$  with an exponent that increases with the order of the EP. This result is independent of the degree of non-Hermiticity  $\alpha$  or the location—left or right—of the EP contour. The

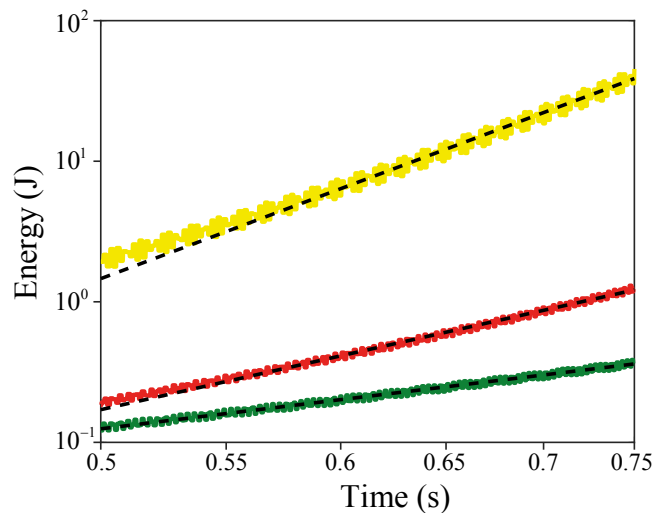


Figure 4. **Energy increase at the EPs.** Unnormalized circuit energy  $E(t)$  on a log-log scale at long times shows linear behavior with a slope that depends on the order  $N$  of the EP. The results are for  $\alpha = 0.2$ , purple (right-side) EP. Similar results are obtained, with appropriate long-time windows, for left- and right-side EP contours for all  $\alpha$ . For the representative data shown, the power-law exponents are 2.62, 4.83, and 8.08, for  $N = 2$ ,  $N = 3$ , and  $N = 5$ , respectively.

large fluctuations in the non-stroboscopic data for  $E(t)$  also hint at the asymmetric dependence of  $E(t)$  on the EP location at a fixed  $\alpha$  [43].

Since the system with  $N$  has an  $N$ th order EP, we expect the unnormalized energy to grow as  $E(t) \propto t^{2(N-1)}$  at long times. To confirm this, Figure 4 shows the system's energy vs time on a log-log scale for  $\alpha = 0.2$ . The slopes obtained from straight-line fits to the log-log data are in agreement with the prediction that the power-law exponent for an EP of order  $N$  is given by  $2(N-1)$  [21, 43].

### IV. CONCLUSION

From their start in quantum theory and mathematical physics, non-Hermitian,  $\mathcal{PT}$ -symmetric models are now studied across the board in fields as widely varied as minimal quantum systems or a single LC oscillator. This veritable cornucopia of experimental realizations has also invited detailed comparison of seemingly different models. Here, we have analyzed one such model, an array of  $N$  inductively coupled RLC circuits with dynamic parameters to show that energy dynamics in it is generated by a  $(3N-1)$ -dimensional non-Hermitian Hamiltonian, and through general formalism, spelled out the constraints that make such Hamiltonian have chiral and  $\mathcal{PT}$  symmetry. We have then shown that this model, with  $2N$  dynamical variables, can be mapped onto an  $N$ -dimensional tight-binding lattice that can support an EP of order  $N$ .

By implementing the gain and loss through a periodic variation of the inductances in the RLC units, we have numerically mapped out the Floquet  $\mathcal{PT}$ -phase diagram for two, three, and five oscillator chains, all of which show EP contours at vanishingly small non-Hermiticities. By tracking the circuit's energy, we are able to extract the order of EP by looking at the power-law-in-time exponent for the  $E(t)$  increase. Our results will be useful for realizing robust, arbitrary-order EPs by means of complex gauge fields in dynamically modulated synthetic oscillator networks.

This work was supported by DGAPA-UNAM under the project UNAM-PAPIIT IN101623, and by CONACYT under the project No. A1-S-8317. J.D.H.-M. thankfully acknowledges financial support by CONACYT. Y.N.J. is supported by ONR Grant No. N00014-21-1-2630.

## Appendix A: Explicit Hamiltonian expressions for two, three, and five oscillator circuits.

### 1. Two coupled RLC oscillators

For two coupled RLC oscillators,  $|\phi(t)\rangle = (V_1, V_2, I_1, I_2, I_{x1})^T$  and the  $5 \times 5$  matrix  $H(t)$  with purely imaginary entries is given by

$$H(t) = i \begin{bmatrix} -\frac{1}{C_1 R_1} & 0 & -\frac{1}{C_1} & 0 & -\frac{1}{C_1} \\ 0 & -\frac{1}{C_2 R_2} & 0 & -\frac{1}{C_2} & \frac{1}{C_2} \\ \frac{1}{L_1(t)} & 0 & 0 & 0 & 0 \\ 0 & \frac{1}{L_2(t)} & 0 & 0 & 0 \\ \frac{1}{L_{12}} & -\frac{1}{L_{12}} & 0 & 0 & 0 \end{bmatrix}. \quad (\text{A1})$$

To generate balanced gain-loss through the temporal modulation of the inductors, we use  $L_1(t) = L_0 e^{f(t)}$  and  $L_2(t) = L_0 e^{-f(t)}$ , and set  $C_{1,2} = C_0$ ,  $L_{12} = 0.5L_0$  and  $R_{1,2} = R_0$ . With  $\gamma(t) = df/dt$ , the circuit Hamiltonian can be written as

$$H_{\text{cir}}(t) = i \begin{bmatrix} -\frac{1}{C_0 R_0} & 0 & -\frac{\omega_0}{e^{f(t)/2}} & 0 & -\frac{\omega_0}{\sqrt{0.5}} \\ 0 & -\frac{1}{C_0 R_0} & 0 & -\frac{\omega_0}{e^{-f(t)/2}} & \frac{\omega_0}{\sqrt{0.5}} \\ \frac{\omega_0}{e^{f(t)/2}} & 0 & \frac{\gamma(t)}{2} & 0 & 0 \\ 0 & \frac{\omega_0}{e^{-f(t)/2}} & 0 & -\frac{\gamma(t)}{2} & 0 \\ \frac{\omega_0}{\sqrt{0.5}} & -\frac{\omega_0}{\sqrt{0.5}} & 0 & 0 & 0 \end{bmatrix}. \quad (\text{A2})$$

### 2. Three coupled RLC oscillators

For three coupled RLC oscillators,  $|\phi(t)\rangle = (V_1, V_2, V_3, I_1, I_2, I_3, I_{x1}, I_{x2})^T$ , and the  $8 \times 8$  matrix  $H(t)$  with purely imaginary entries is given by

$$H(t) = i \begin{bmatrix} -\frac{1}{C_1 R_1} & 0 & 0 & -\frac{1}{C_1} & 0 & 0 & -\frac{1}{C_1} & 0 \\ 0 & -\frac{1}{C_2 R_2} & 0 & 0 & -\frac{1}{C_2} & 0 & \frac{1}{C_2} & -\frac{1}{C_2} \\ 0 & 0 & -\frac{1}{C_3 R_3} & 0 & 0 & -\frac{1}{C_3} & 0 & \frac{1}{C_3} \\ \frac{1}{L_1(t)} & 0 & 0 & 0 & 0 & 0 & 0 & 0 \\ 0 & \frac{1}{L_2} & 0 & 0 & 0 & 0 & 0 & 0 \\ 0 & 0 & \frac{1}{L_3(t)} & 0 & 0 & 0 & 0 & 0 \\ \frac{1}{L_{x1}} & -\frac{1}{L_{x1}} & 0 & 0 & 0 & 0 & 0 & 0 \\ 0 & \frac{1}{L_{x2}} & -\frac{1}{L_{x2}} & 0 & 0 & 0 & 0 & 0 \end{bmatrix}. \quad (\text{A3})$$

To maintain  $\mathcal{PT}$ -symmetry and generate balanced gain and loss, we use  $L_{x1} = L_{x2} = 0.5L_0$ ,  $L_1(t) = L_0 e^{f(t)}$ ,

$L_2 = L_0$  and  $L_3(t) = L_0 e^{-f(t)}$ . The resulting circuit Hamiltonian becomes



- 
- [1] C. M. Bender and S. Boettcher, Real spectra in non-Hermitian Hamiltonians having  $\mathcal{PT}$  symmetry, *Phys. Rev. Lett.* **80**, 5243 (1998).
- [2] C. M. Bender, S. Boettcher, and P. N. Meisinger,  $\mathcal{PT}$ -symmetric quantum mechanics, *J. Math. Phys.* **40**, 2201 (1999).
- [3] C. M. Bender, Introduction to  $\mathcal{PT}$ -symmetric quantum theory, *Contemp. Phys.* **46**, 277 (2005).
- [4] G. Lévai and M. Znojil, Systematic search for  $\mathcal{PT}$ -symmetric potentials with real energy spectra, *J. Phys. A: Math. Gen.* **33**, 7165 (2000).
- [5] J. D. Huerta Morales, J. Guerrero, S. López-Aguayo, and B. M. Rodríguez-Lara, Revisiting the optical  $\mathcal{PT}$ -symmetric dimer, *Symmetry* **8**, 83 (2016).
- [6] A. Guo, G. J. Salamo, D. Duchesne, R. Morandotti, M. Volatier-Ravat, V. Aimez, G. A. Siviloglou, and D. N. Christodoulides, Observation of  $\mathcal{PT}$ -symmetry breaking in complex optical potentials, *Phys. Rev. Lett.* **103**, 093902 (2009).
- [7] C. E. Rüter, K. G. Makris, R. El-Ganainy, D. N. Christodoulides, M. Segev, and D. Kip, Observation of parity–time symmetry in optics, *Nature Phys.* **6**, 192 (2010).
- [8] L. Feng, R. El-Ganainy, and L. Ge, Non-Hermitian photonics based on parity–time symmetry, *Nature Photon.* **11**, 752 (2017).
- [9] R. El-Ganainy, K. G. Makris, M. Khajavikhan, Z. H. Musslimani, S. Rotter, and D. N. Christodoulides, Non-Hermitian physics and  $\mathcal{PT}$  symmetry, *Nature Phys.* **14**, 11 (2018).
- [10] H. Eleuch and I. Rotter, Clustering of exceptional points and dynamical phase transitions, *Phys. Rev. A* **93**, 042116 (2016).
- [11] S. K. Özdemir, S. Rotter, F. Nori, and L. Yang, Parity–time symmetry and exceptional points in photonics, *Nat. Mater.* **18**, 783 (2019).
- [12] M. Sakhdari, M. Hajizadegan, Q. Zhong, D. N. Christodoulides, R. El-Ganainy, and P.-Y. Chen, Experimental observation of  $\mathcal{PT}$  symmetry breaking near divergent exceptional points, *Phys. Rev. Lett.* **123**, 193901 (2019).
- [13] H. Hodaie, A. U. Hassan, S. Wittek, H. Garcia-Gracia, R. El-Ganainy, D. N. Christodoulides, and M. Khajavikhan, Enhanced sensitivity at higher-order exceptional points, *Nature* **548**, 187 (2017).
- [14] W. Chen, S. K. Özdemir, G. Zhao, J. Wiersig, and L. Yang, Exceptional points enhance sensing in an optical microcavity, *Nature* **548**, 192 (2017).
- [15] Y. Huang, Y. Shen, and G. Veronis, Non- $\mathcal{PT}$ -symmetric two-layer cylindrical waveguide for exceptional-point-enhanced optical devices, *Opt. Express* **27**, 37494 (2019).
- [16] M. I. Rosa, M. Mazzotti, and M. Ruzzene, Exceptional points and enhanced sensitivity in  $\mathcal{PT}$ -symmetric continuous elastic media, *J. Mech. Phys. Solids* **149**, 104325 (2021).
- [17] I. Rotter, A non-Hermitian Hamilton operator and the physics of open quantum systems, *J. Phys. A: Math. Theor.* **42**, 153001 (2009).
- [18] M. Müller and I. Rotter, Exceptional points in open quantum systems, *J. Phys. A: Math. Theor.* **41**, 244018 (2008).
- [19] M. H. Teimourpour, Q. Zhong, M. Khajavikhan, and R. El-Ganainy, in *Parity-time Symmetry and Its Applications*, edited by D. Christodoulides and J. Yang (Springer Singapore, Singapore, 2018) pp. 261–275.
- [20] W. D. Heiss, The physics of exceptional points, *J. Phys. A: Math. Theor.* **45**, 444016 (2012).
- [21] M. A. Quiroz-Juárez, A. Perez-Leija, K. Tschernig, B. M. Rodríguez-Lara, O. S. Magaña-Loaiza, K. Busch, Y. N. Joglekar, and R. de J. León-Montiel, Exceptional points of any order in a single, lossy waveguide beam splitter by photon-number-resolved detection, *Photon. Res.* **7**, 862 (2019).
- [22] S. M. Zhang, X. Z. Zhang, L. Jin, and Z. Song, High-order exceptional points in supersymmetric arrays, *Phys. Rev. A* **101**, 033820 (2020).
- [23] M. Y. Nada and F. Capolino, Exceptional point of sixth-order degeneracy in a modified coupled-resonator optical waveguide, *Journal of the Optical Society of America B* **37**, 2319 (2020).
- [24] J. Wiersig, Enhancing the sensitivity of frequency and energy splitting detection by using exceptional points: Application to microcavity sensors for single-particle detection, *Phys. Rev. Lett.* **112**, 203901 (2014).
- [25] Z. P. Liu, J. Zhang, S. K. Özdemir, B. Peng, H. Jing, X. Y. Lü, C. W. Li, L. Yang, F. Nori, and Y. X. Liu, Metrology with  $\mathcal{PT}$ -symmetric cavities: Enhanced sensitivity near the  $\mathcal{PT}$ -phase transition, *Phys. Rev. Lett.* **117**, 110802 (2016).
- [26] N. Moiseyev and M. Šindelka, Transfer of information through waveguides near an exceptional point, *Phys. Rev. A* **103**, 033518 (2021).
- [27] B. Peng, S. K. Özdemir, F. Lei, F. Monifi, M. Gianfreda, G. L. Long, S. Fan, F. Nori, C. M. Bender, and L. Yang, Parity–time-symmetric whispering-gallery microcavities, *Nature Phys.* **10**, 394 (2014).
- [28] H. Jing, S. K. Özdemir, H. Lü, and F. Nori, High-order exceptional points in optomechanics, *Sci. Rep.* **7**, 3386 (2017).
- [29] B. Jaramillo-Ávila, C. Ventura-Velázquez, R. de J. León-Montiel, Y. N. Joglekar, and B. M. Rodríguez-Lara,  $\mathcal{PT}$ -symmetry from Lindblad dynamics in a linearized optomechanical system, *Scientific Reports* **10**, 1761 (2020).
- [30] W. Xiong, Z. Li, Y. Song, J. Chen, G. Q. Zhang, and M. Wang, Higher-order exceptional point in a pseudo-Hermitian cavity optomechanical system, *Phys. Rev. A* **104**, 063508 (2021).
- [31] F. Quijandría, U. Naether, S. K. Özdemir, F. Nori, and D. Zueco,  $\mathcal{PT}$ -symmetric circuit QED, *Phys. Rev. A* **97**, 053846 (2018).
- [32] Z. Bian, L. Xiao, K. Wang, X. Zhan, F. A. Onanga, F. Ruzicka, W. Yi, Y. N. Joglekar, and P. Xue, Conserved quantities in parity-time symmetric systems, *Phys. Rev. Research* **2**, 022039 (2020).
- [33] C. Shi, M. Dubois, Y. Chen, L. Cheng, H. Ramezani, Y. Wang, and X. Zhang, Accessing the exceptional points of parity-time symmetric acoustics, *Nat. Commun.* **7**, 11110 (2016).
- [34] K. Ding, G. Ma, M. Xiao, Z. Q. Zhang, and C. T. Chan, Emergence, coalescence, and topological properties of multiple exceptional points and their experimental re-



- alization, *Phys. Rev. X* **6**, 021007 (2016).
- [35] S. Wang, B. Hou, W. Lu, Y. Chen, Z. Q. Zhang, and C. T. Chan, Arbitrary order exceptional point induced by photonic spin-orbit interaction in coupled resonators, *Nat. Commun.* **10**, 832 (2019).
- [36] J. Schindler, A. Li, M. C. Zheng, F. M. Ellis, and T. Kottos, Experimental study of active LRC circuits with  $\mathcal{PT}$  symmetries, *Phys. Rev. A* **84**, 040101 (2011).
- [37] Z. Lin, J. Schindler, F. M. Ellis, and T. Kottos, Experimental observation of the dual behavior of  $\mathcal{PT}$ -symmetric scattering, *Phys. Rev. A* **85**, 050101 (2012).
- [38] H. Kazemi, M. Y. Nada, T. Mealy, A. F. Abdelshafy, and F. Capolino, Exceptional points of degeneracy induced by linear time-periodic variation, *Phys. Rev. Appl.* **11**, 014007 (2019).
- [39] H. Kazemi, M. Y. Nada, A. Nikzamir, F. Maddaleno, and F. Capolino, Experimental demonstration of exceptional points of degeneracy in linear time periodic systems and exceptional sensitivity, *Journal of Applied Physics* **131**, 144502 (2022).
- [40] A. Stegmaier, S. Imhof, T. Helbig, T. Hofmann, C. H. Lee, M. Kremer, A. Fritzsche, T. Feichtner, S. Klemmt, S. Höfling, I. Boettcher, I. C. Fulga, L. Ma, O. G. Schmidt, M. Greiter, T. Kiessling, A. Szameit, and R. Thomale, Topological defect engineering and  $\mathcal{PT}$  symmetry in non-Hermitian electrical circuits, *Phys. Rev. Lett.* **126**, 215302 (2021).
- [41] X. Yang, J. Li, Y. Ding, M. Xu, X.-F. Zhu, and J. Zhu, Observation of transient parity-time symmetry in electronic systems, *Phys. Rev. Lett.* **128**, 065701 (2022).
- [42] W. Cao, C. Wang, W. Chen, S. Hu, H. Wang, L. Yang, and X. Zhang, Fully integrated parity-time-symmetric electronics, *Nature Nanotechnology* **17**, 262 (2022).
- [43] M. A. Quiroz-Juárez, K. S. Agarwal, Z. A. Cochran, J. L. Aragón, Y. N. Joglekar, and R. de J. León-Montiel, On-demand parity-time symmetry in a lone oscillator through complex synthetic gauge fields, *Phys. Rev. Appl.* **18**, 054034 (2022).
- [44] Y. N. Joglekar, C. Thompson, D. D. Scott, and G. Vemuri, Optical waveguide arrays: quantum effects and  $\mathcal{PT}$  symmetry breaking, *The European Physical Journal Applied Physics* **63**, 30001 (2013).
- [45] A. Perez-Leija, R. Keil, H. Moya-Cessa, A. Szameit, and D. N. Christodoulides, Perfect transfer of path-entangled photons in  $J_x$  photonic lattices, *Phys. Rev. A* **87**, 022303 (2013).
- [46] S. Weimann, A. Perez-Leija, M. Lebugle, R. Keil, M. Tichy, M. Gräfe, R. Heilmann, S. Nolte, H. Moya-Cessa, G. Weihs, D. N. Christodoulides, and A. Szameit, Implementation of quantum and classical discrete fractional Fourier transforms, *Nat. Commun.* **7**, 11027 (2016).
- [47] M. A. Quiroz-Juárez, C. You, J. Carrillo-Martínez, D. Montiel-Álvarez, J. L. Aragón, O. S. Magaña Loaiza, and R. de J. León-Montiel, Reconfigurable network for quantum transport simulations, *Phys. Rev. Res.* **3**, 013010 (2021).
- [48] K. Tschernig, R. de J. León-Montiel, O. S. Magaña-Loaiza, A. Szameit, K. Busch, and A. Perez-Leija, Multiphoton discrete fractional Fourier dynamics in waveguide beam splitters, *J. Opt. Soc. Am. B* **35**, 1985 (2018).
- [49] R. de J. León-Montiel, M. A. Quiroz-Juárez, J. L. Domínguez-Juárez, R. Quintero-Torres, J. L. Aragón, A. K. Harter, and Y. N. Joglekar, Observation of slowly decaying eigenmodes without exceptional points in Floquet dissipative synthetic circuits, *Commun. Phys.* **1**, 88 (2018).
- [50] Y. N. Joglekar, R. Marathe, P. Durganandini, and R. K. Pathak,  $\mathcal{PT}$  spectroscopy of the Rabi problem, *Phys. Rev. A* **90**, 040101 (2014).